Supporting information

Drastically Increased Electrical and Thermal Conductivities of Pt-infiltrated MXene

Viet Phuong Nguyen,[a,b] Mikyung Lim,[b] Kyung-Shik Kim,[b] Jae-Hyun Kim,[a,b] Ji Su Park,[c] Jongmin Yuk,[c] Seung-Mo Lee[a,b,*]

[a] Nanomechatronics, Korea University of Science and Technology (UST), Daejeon 34113, Republic of Korea

[b] Department of Nanomechanics, Korea Institute of Machinery and Materials (KIMM), Daejeon 34103, Republic of Korea

[c] Department of Materials Science and Engineering, Korea Advanced Institute of Science and Technology, 335 Science Road, Daejeon 34141, Republic of Korea

* Corresponding author: sm.lee@kimm.re.kr

1. Experimental section

Preparation of Ti_3C_2 films

1 g Ti_3C_2 powder (purchased from Invisible, South Korea) was intercalated by dimethyl sulfoxide (DMSO) under magnetic stirring for 24h. After intercalation, the intercalated powder was separated from excess DMSO by centrifugation at 3500 rpm. The solution containing intercalated powders was sonicated and centrifuged to obtain a few-layer Ti_3C_2 colloidal solution. The concentration of MXene solution was determined by filtering a certain amount of solution. Finally, the MXene film (rTi_3C_2) was fabricated by vacuum filtration of the colloidal solution of MXene nanosheets with an Anodisc™ 47 membrane, followed by drying at room temperature in a vacuum overnight.

Preparation of Ti_3C_2/Pt films

The as-prepared free-standing Ti_3C_2 films were loaded into an ALD chamber (S100, Savannah, Cambridge NanoTech Inc.) for Pt infiltration using (Methylcyclopentadienyl)trimethylplatinum ($MeCpPtMe_3$) and O_2 as precursors. The ALD process condition was optimized and set in the exposure mode with 0.1 s pulse, 40 s exposure, and 60 s purging of $MeCpPtMe_3$, followed by 0.05 s pulse, 10 s exposure, and 30 s purging of O_2 for each ALD cycle at a constant N_2 flow rate of 20 sccm. The process temperature and pressure were set at 150 °C and ~0.1 Torr, c. Pt ALD was applied to Ti_3C_2 MXene films (100 ALD cycles). The growth rate of Pt on a reference Si substrate was measured as 0.4 Å/cycle.

Material characterizations

The analysis of the morphology and the element was performed using FE-SEM (JSM-7800F, JEOL) and EDX (Oxford AZtec® EDX system), respectively. AFM images of the MXene nanosheet were obtained using an XE-100 system (Park systems) in the non-contact mode. For TEM investigation, Tecnai F30 (FEI at 300 kV) was used. XRD spectra were recorded using Empyrean diffractometer (PANalytical with Cu Kα (λ = 1.5418 Å)). XPS spectra were obtained using MultiLab 2000 (Thermo Fisher Scientific with an Al Kα X-ray source). Raman spectra were acquired using inVia Raman microscope equipped with 514 nm-laser (x50, Renishaw). The contact angle measurements were carried out using DSA 100 (Krüss GmbH, Hamburg, Germany).

Characterizations of thermal properties

The in-plane thermal conductivity ($K_{//}$) was calculated according to the formula: $K_{//} = \alpha.C_p.\rho$, where α was the thermal diffusivity which was obtained from LaserPIT-M2 (Ulvac), C_p was the specific heat capacity which was measured by DSC SDT Q600 (TA Instruments), and ρ was the density of the sample which was determined by the Archimedes law. The cross-plane

thermal conductivity ($K_{\perp}$) was determined using time-domain thermoreflectance (Transometer^{TM} N8 system, TMX Scientific, Inc) at room temperature. At least ten measurements were conducted for each sample.

Characterizations of electrical properties

The in-plane electrical conductivity was investigated by an Agilent B1500A semiconductor device parameter analyzer with a 4-point Au probe. Films were cut into 3 mm x 20 mm rectangular strips. To avoid contact resistance, 200-nm gold was coated on the sample strips where the probes contacted the samples. The distance between two consecutive probes was 3 mm. The voltage between two inner probes was recorded when a direct current changing from -1 mA to 1 mA was applied on two outer probes. The in-plane electrical conductivity ($\sigma_{//}$) was calculated according to the formula: $\sigma_{//} = L/(S \cdot R_{//})$, where L, S, and $R_{//}$ were the distance between two inner probes, the cross-sectional area of the samples, the in-plane resistance of the samples, respectively. $R_{//}$ was obtained from the slope of the V-I curve. The cross-plane electrical conductivity was examined by a standard electrochemical workstation. The films were coated with 200-nm gold on both sides, then cut into the 0.5 cm x 0.5 cm pieces and inserted into the 2-electrode cell. The current was recorded by the linear sweep voltammetry mode with the voltage range from -0.1 V to 0.1 V and a scan rate of 10 mV/s. The cross-plane electrical conductivity ($\sigma_{\perp}$) was calculated according to the formula: $\sigma_{\perp} = d/(A \cdot R_{\perp})$, where d, A, and $R_{\perp}$ were the thickness of the samples, the sample area of the samples, and the cross-plane resistance of the samples, respectively. $R_{\perp}$ was obtained from the slope of the V-I curve. Variation in electrical resistance during the cyclic bending test was measured by a source meter (Keithley source meter 2400, Keithley Instruments). A commercial mechanical tester (Tytron 250, MTS) was employed for doing the cyclic bending test. An electrode of 2 × 20 mm^2 was attached on a PET substrate of 5 × 60 mm^2, which was then gripped by the two ends of

the mechanical tester. The servo-electric actuator linearly moved in the displacement range of 10 mm at a frequency of 1 Hz up to 1000 cycles was used.

Characterizations of mechanical properties

The mechanical properties of rTi_3C_2, aTi_3C_2, and Ti_3C_2/Pt films were measured using a microtester (Deben, N200) equipped with a 2 kN load cell. These films were cut into rectangular strips with a dimension of 2 mm x 20 mm using a razor blade. The gap between clamps and displacement rate was set at 12 mm and 1.5 μm/s, respectively. The specimens were continuously extended until a fracture occurred. At least six tests were conducted for each sample.

Electrothermal conversion performance

Electrical-to-heat conversion performance was tested through the construction of simple heaters from the MXene-based films. Films with a size of 10 x 20 mm^2 were pasted on glass substrates and connected with two copper foils by silver paste. Different DC voltages were supplied by a source meter (Keithley 2420). An infrared camera (FLIR-300 series, FLIR System, Inc.) calibrated by a thermocouple was used to visualize the temperature distribution of the heater surface.

2. Supporting figures

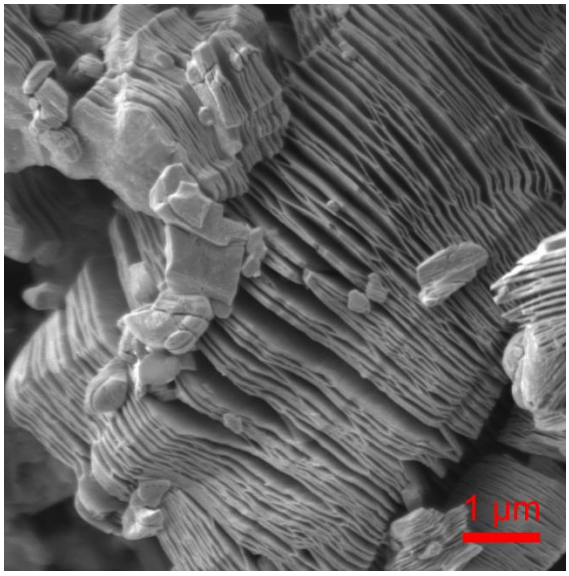

Fig. S1 SEM image of the MXene powder (Ti_3C_2).

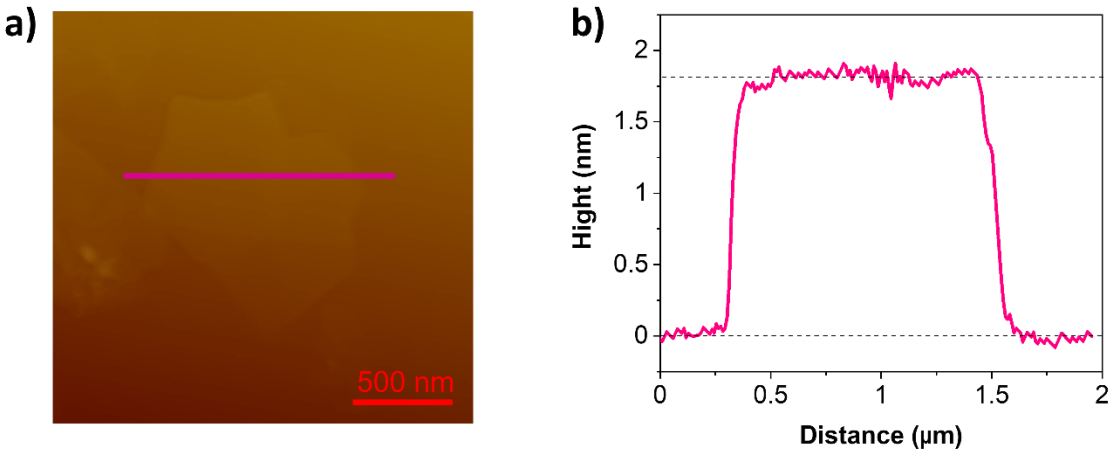

Fig. S2 AFM image of (a) the Ti_3C_2 nanosheets and (b) corresponding height profile.

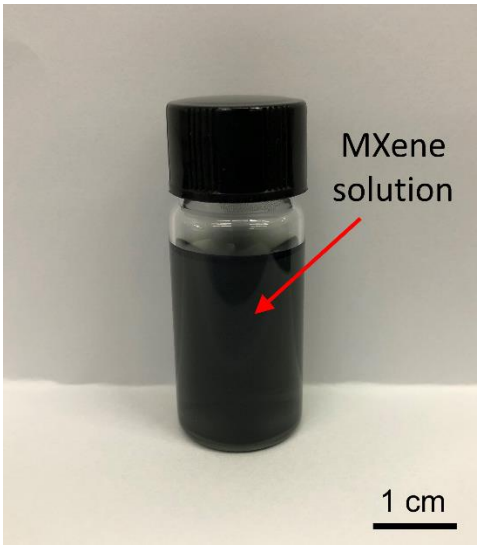

Fig. S3 MXene solution with high stability.

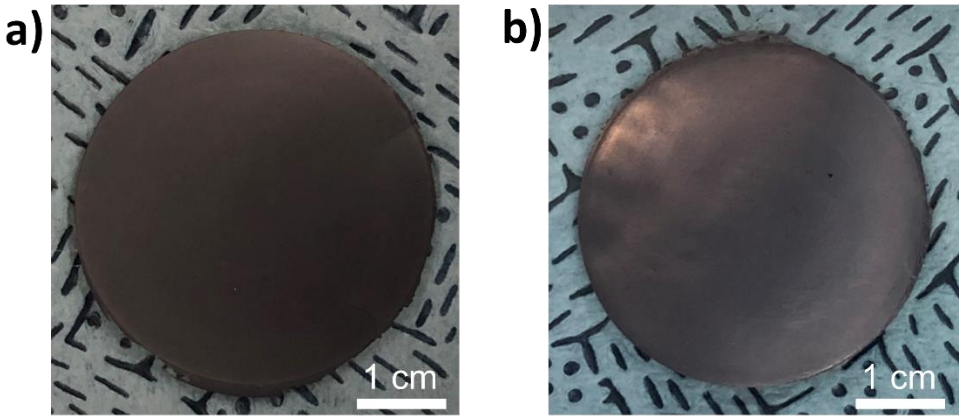

Fig. S4 Optical microscope images of (a) the raw MXene (rTi_3C_2) and (b) the Pt-infiltrated MXene (Pt/Ti_3C_2) film.

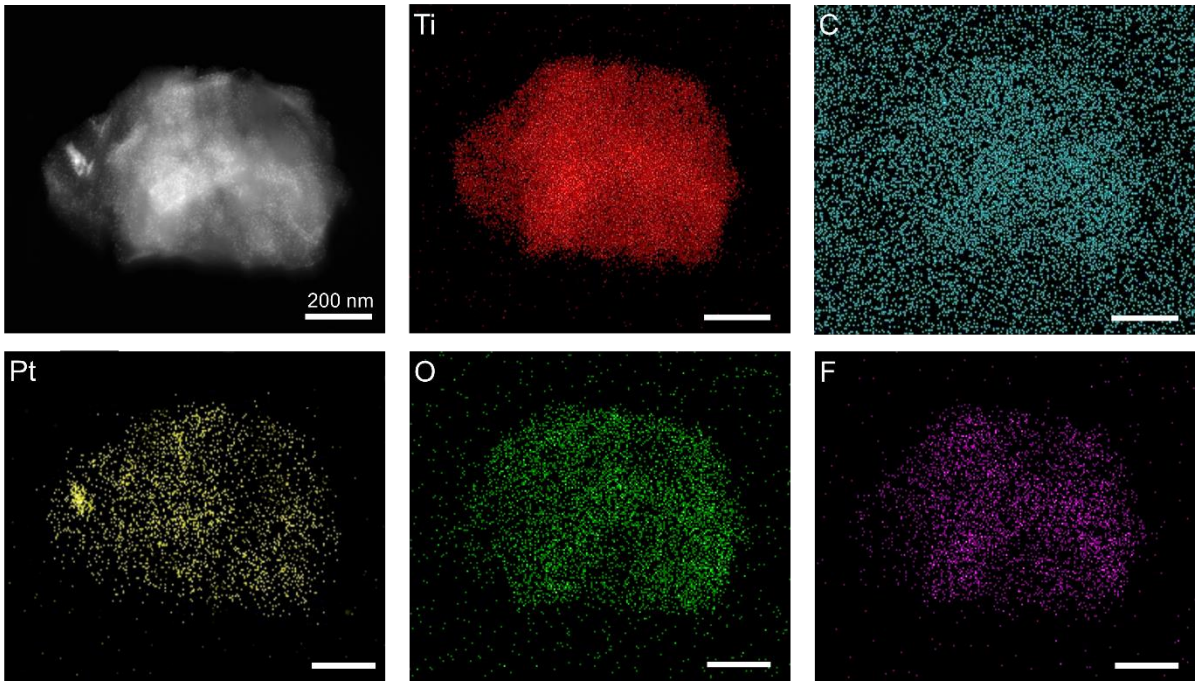

Fig. S5 TEM-EDX mapping images of Ti, C, Pt, O, F elements existing in the Pt-infiltrated MXene films.

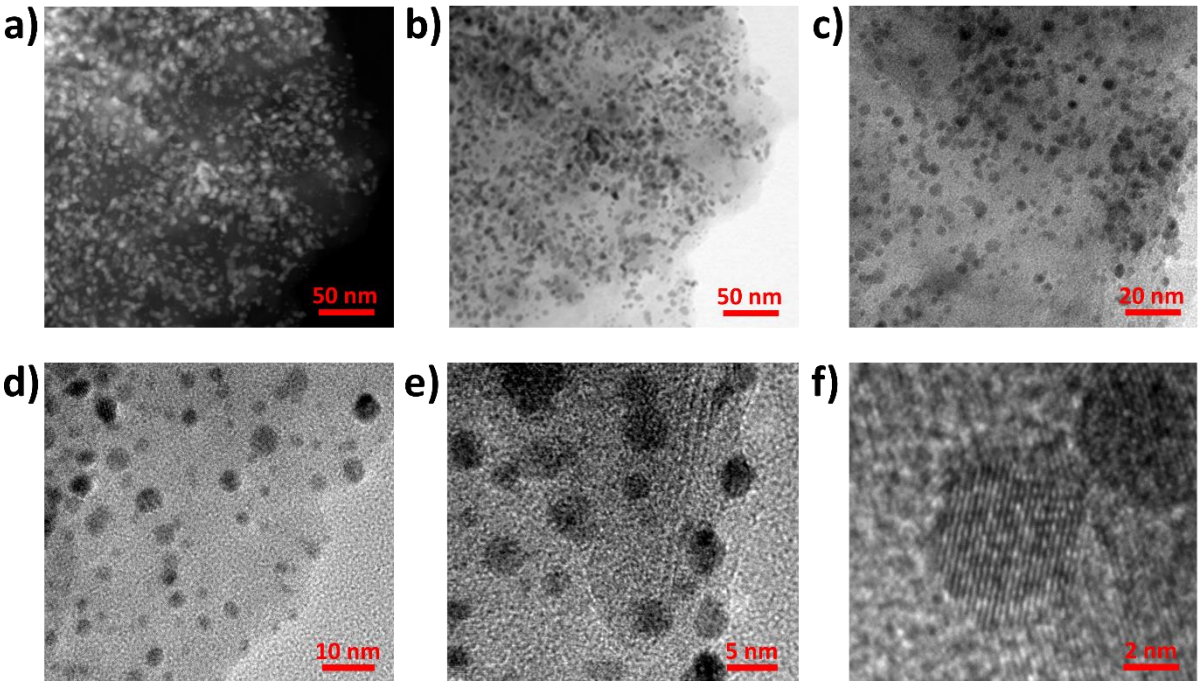

Fig. S6 DF-TEM (a) and HR-TEM (b-f) images of the Pt-infiltrated MXene films at various resolutions.

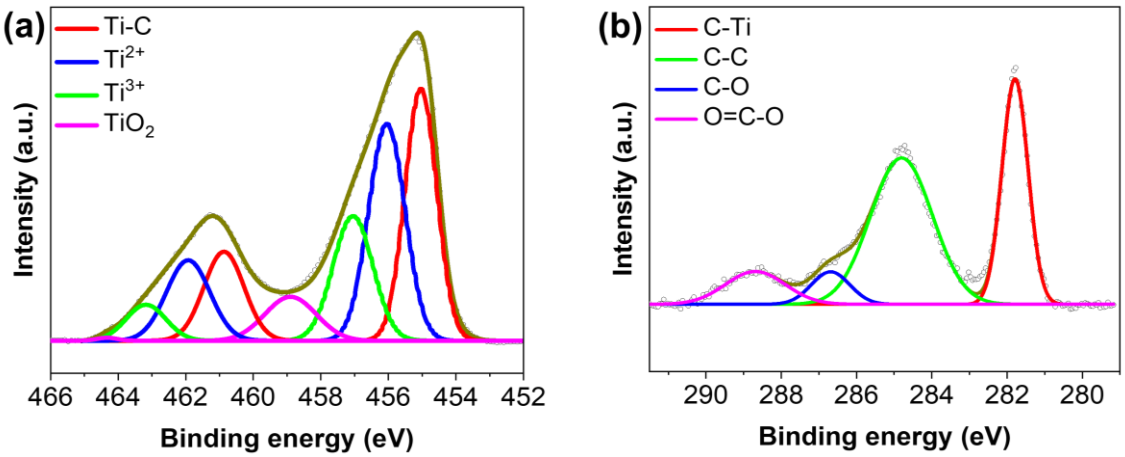

c

Fig. S7 High-resolution XPS Ti 2p and C 1s of the annealed MXene films (aTi_3C_2).

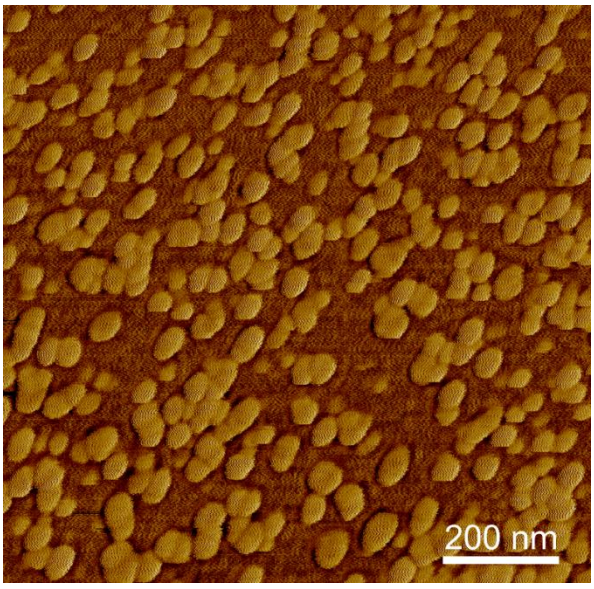

Fig. S8 AFM image of Pt islands formed on the surface of the Si substrate after 100-cycle ALD.

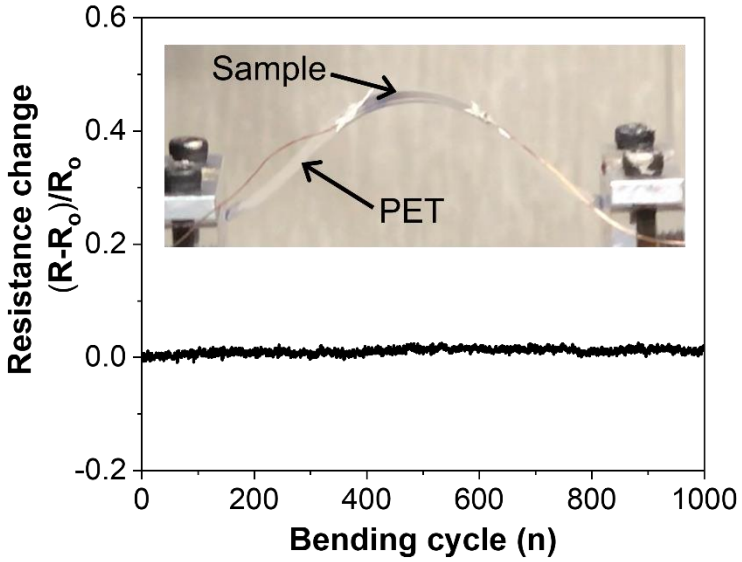

Fig. S9 Electrical resistance changes $(R - R_o)/R_o$ of the Pt-infiltrated MXene films under cyclic bending test for 1000 cycles. No significant change was observed.

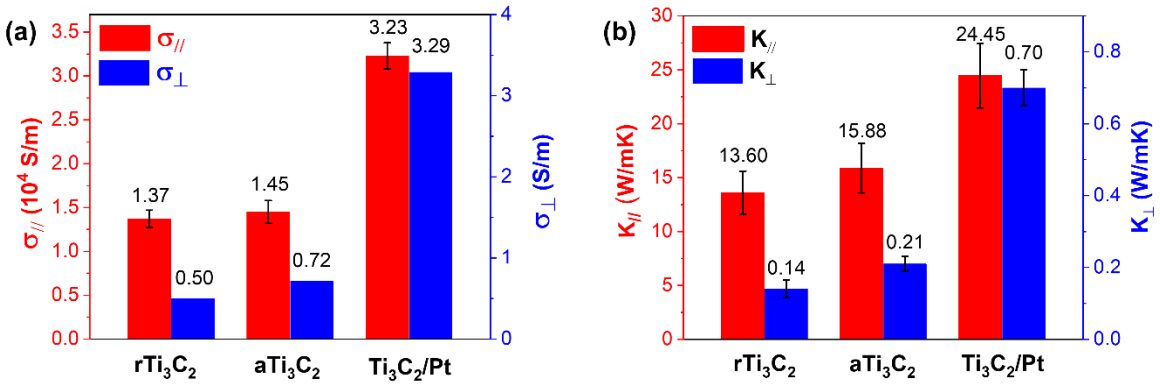

Fig. S10 Summary of (a) electrical and (b) thermal conductivities of the MXene-based films.

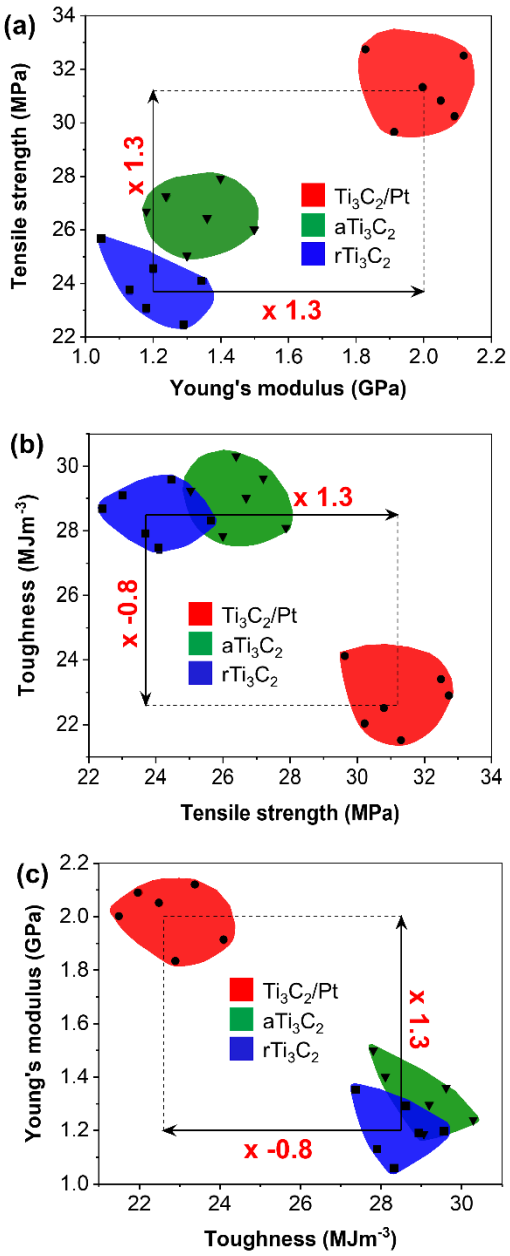

Fig. S11 Summary of mechanical properties of the MXene-based films. (a) A chart of tensile strength and Young's modulus. (b) A chart of toughness and tensile strength. (c) A chart of toughness and Young's modulus. The toughness can be defined as the amount of energy per unit volume that a material can absorb before rupturing. In this work, the toughness was estimated by calculating the area under the stress-strain curve of each MXene samples, i.e. $\int_0^{\epsilon_f} \sigma d\epsilon$, where ε, ε_f, and σ are the strain, the strain upon failure, and the stress, respectively.

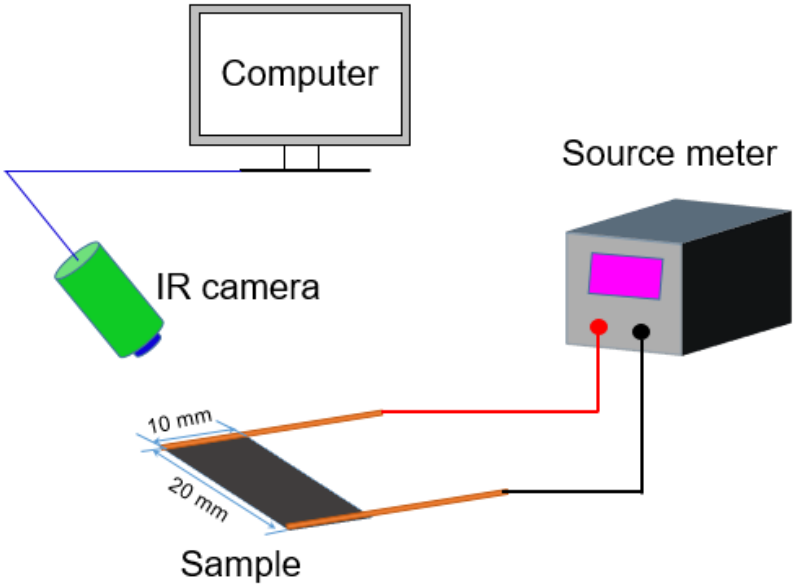

Fig. S12 Schematic illustration showing the setup of the electrothermal performance of the heaters.

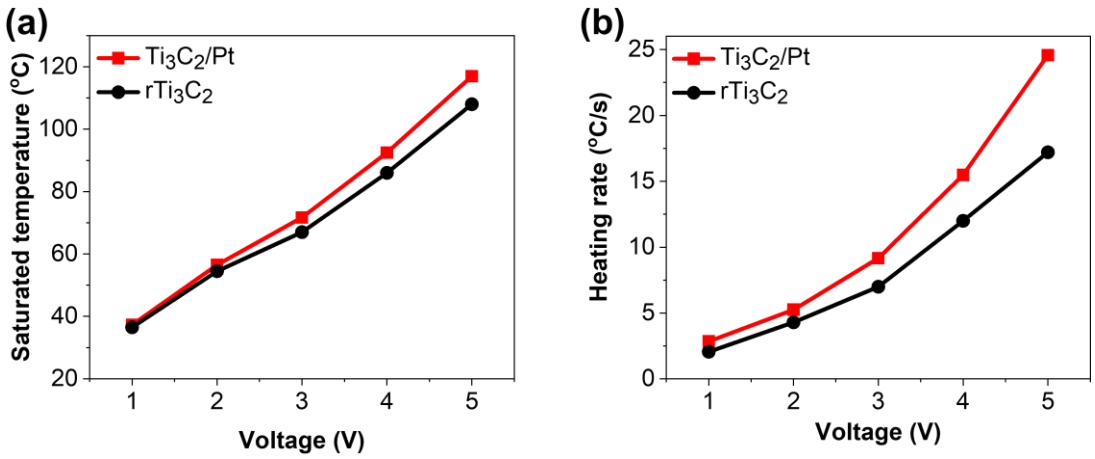

Fig. S13 Summary of (a) the saturated temperature and (b) the heating rate of the MXene-based heaters at different voltages. The heater made by the Pt-infiltrated MXene shows higher performance than the raw MXene.

Table S1 Atom atomic percent of elements existing in the MXene-based films (unit.: at.%)

Sample	Ti	C	O	F	Pt
rTi_3C_2	45.05	33.61	12.76	8.58	0
Ti_3C_2/Pt	44.97	33.75	11.82	8.31	1.15

Table S2 Comparison of the thermal conductivities of the Ti_3C_2 MXene from literature

Sample	$K_{//}$		$K_{\perp}$		Ref.
	Value (W/mK)	Enhancement (times)	Value (W/mK)	Enhancement (times)	
Ti_3C_2/MMT	28.8	1.88	0.27	-0.84	49
Ti_3C_2/PVA	4.57	/	/	/	50
Ti_3C_2/CNF	11.57	/	1.25	/	51
Ti_3C_2/Pt	24.45	1.8	0.7	5.0	This work

- indicates a decrease.

/ indicates that the values are either not available or impossible to be calculated.